FAST EXTRACTION OF DEBUNCHED AGS BEAM*

L.N. Blumberg, J.G. Cottingham, J.W. Glenn, J.J. Grisoli,
M. Month and A. van Steenbergen
Brookhaven National Laboratory
Upton, New York

Summary

A new system for fast extraction of the AGS beam is described in which the beam is moved rapidly across a hyper thin septum (HTS) and deflected into the aperture of a thin-septum ejection magnet (EM). The effects of momentum spread on the clearance obtained at the ejector septum are calculated. Orbit deformations from $\lambda/2$ backleg winding bumps centered at the septum and ejector azimuths are calculated and the effects of these perturbations on orbits near the $\nu_H = 9$ resonance are discussed. Loss calculations for an electrostatic HTS indicate that proton losses will be 0.1% per turn for a .002 in. diam. tungsten wire array or 0.8% per turn for a .002 in. copper foil. The ferrite beam kickers required for the fast deformation at the HTS are described. Component parameters for fractional extraction are: C15 and E15 beam kickers = .75 mrad, E10 HTS = 1.2 mrad, H10 EM = 22 mrad, and I10 EM = 21 mrad. Results of initial tests with a 2.25 m electrostatic septum of .1 mm diam. tungsten wires at 2 mm spacing are discussed.

I. Introduction

The method of fast extraction used heretofore[1,2] at the AGS involved the deflection of a single bunch from the synchrotron. The spill duration, $\sim$ 10 ns, was well within the 2.5 μs interval during which the rf separators are energized, and the quantity of beam, $\sim 1.5\times10^{11}$ protons per bunch, was appropriate to attain the desired $\sim$ 10 secondaries per extraction required for bubble chamber pictures. For the AGS after conversion, however, we anticipate $\sim 10^{12}$ protons per bunch with the bubble chambers capable of up to 4 expansions per AGS cycle at 100 ms intervals. To satisfy these requirements, the conventional bunched extraction method will be wasteful both of protons and flat top time since the beam would have to remain bunched for approximately 1/3 of the 1 sec flat top, during which the slow resonant spill would be inoperative. (Counter experiments using the slow external beam (SEB) require a debunched beam.) There are, moreover, problems associated with components for single bunch extraction of the post-Conversion beam relating to the expected factor of two larger emittances: the fast kicker amplitude and the apertures in internal and external transport magnets would increase by $\sqrt{2}$. To overcome these difficulties an extraction method is planned in which the SEB is interrupted for $\sim$ 10 ms intervals on the flat top, during which fast external beam (FEB) orbit deformations and beam kickers are energized to move the circulating, debunched beam across a thin septum. Since the rise and fall time of the beam kicker is not constrained to the $\sim$ 200 ns interval between bunches, the power supply for this component is considerably simplified. Moreover, since only a fraction of the beam cross section is "shaved" by this method, the emittance of the external beam is smaller than that of the circulating beam, which means smaller spot size at experimental targets. The duration of the spill is controlled by the amount of azimuth "shaved" and the quantity of extracted protons depends on the product of the spill duration and the amplitude of the "bite" of transverse phase space. The new method thus provides greater operational flexibility and relaxes the constraint on bubble chamber recycling time.

In Fig. 1 we show the location of the various elements of the system: backleg windings about selected magnets to produce orbit deformations at the septum and ejector magnets, beam kickers to produce a fast ($\gtrsim$ 1.75 μsec), 3/2 λ deformation with peak amplitude near the thin septum straight section, and a thin-septum ejector magnet at H10 which can either deflect the beam out to the new North Experimental Area or inward to the I10 ejector magnet for the existing 80-in. Bubble Chamber beam. The deformed orbit and trajectory of the central ray deflected by the beam kickers are also shown. Special vacuum chambers are required to accommodate the large outward excursion near the ejector magnets.

II. Location and Required Deflection For Thin Septum

The choice of location for components was based on several criteria: (1) minimum deflection requirement for the HTS, (2) desire to keep SEB components at present locations, (3) minimum number of rf stations displaced, (4) desire to maintain FEB components for bunched extraction at present locations, and (5) suitability of location for construction of service buildings. Both 2-stage (thin septum plus ejector) and 3-stage (thin septum, intermediate septum and ejector) systems were considered. Of four possible 2-stage systems, E10 → H10 required the least HTS deflection angle. Of seven possible 3-stage systems, only B20 → C5 → H10 satisfied all of the criteria. The deflections required for B20 and E10 were 1.06 and 1.17 mrad, respectively. We did not regard this difference as sufficiently large to justify the added complexity of the 3-stage system.

The deflection required for the E10 septum can be obtained from linear theory if we assume that the betatron phase shift Ψ from E10 to H10 is independent of momentum. The transport matrix is then [3]

$$M = \begin{pmatrix} \cos\Psi + \alpha\sin\Psi & \beta\sin\Psi \\ -\gamma\sin\Psi & \cos\Psi - \alpha\sin\Psi \end{pmatrix} \qquad (1)$$

with $\alpha = 1.284$ and $\beta = 603$ in. from AGS orbit calculations,[4] $\gamma = (1+\alpha^2)/\beta$, and $\Psi \approx 61^\circ$. For the E10 septum at distance d from the center of an ellipse containing particles of momentum p_{max} the position at H10 of points on the E10 septum, designated 1 and 2 in Fig. 2, after deflection k is

$$x_{1,2} = d\cos\Psi + \beta k\sin\Psi \pm \sin\Psi\sqrt{x_m^2 - d^2} \qquad (2)$$

where the + refers to point 1, $x_m = \sqrt{\epsilon\beta}$ is the ellipse half-width, and the emittance $E = \pi\epsilon = .1\ \pi$ inch-mrad is approximately twice the present[5] AGS horizontal value. The "shaved" portion of the ellipse between $x = d$ and $x = x_m$ in Fig. 2 also contains protons of lower momentum with equilibrium orbits on the line $x'_{EO} = -(\alpha/\beta)\,x_{EO}$. If we designate by 1′ and 2′ the intersections with the septum of an ellipse centered at $x = -D$ and of momentum $p' < p_{max}$, then the position of these points at H10 is given using Eq. (1) as

$$x_{1',2'} = (d+D)\cos\Psi + \beta k\sin\Psi - D \pm \sin\Psi\sqrt{x_m^2 - (d+D)^2}. \qquad (3)$$

If we form the difference $f(D,d) = x_{2'} - x_2$ and set $(\partial f/\partial D)_{D=0} = 0$ we obtain the critical septum position $d_c = x_m \sin\Psi/2$ such that, for $d > d_c$, we have $x_{2'} > x_2$ and the separation S between the deflected and undeflected beam at H10 is just $x_{2'} - x_m$. For $d < d_c$ we can show that $f(D,d)$ has a minimum at $D_m = d_c - d$ such that $x_{2'} < x_2$ and the separation is then decreased by momentum spread. For the two cases

*Work supported by the U.S. Atomic Energy Commission.

$$S = d\cos\Psi + \beta k \sin\Psi - x_m - \sin\Psi\sqrt{x_m^2 - d^2} \quad d > d_c$$

$$S = -x_m - 2d_c + d + \beta k \sin\Psi \quad d < d_c. \tag{4}$$

We plan to operate the beam with the septum position $d \approx 0$ (beam "bite" $\approx x_m$) which, for the AGS, corresponds to a momentum bite $\Delta p/p \approx .3\%$. The total momentum spread in the AGS beam during flat top however, is, $\sim .6\%$ (momentum spread is introduced to debunch the beam[5] for the SEB and prevent rebunching). Therefore, if we require a larger beam bite we will ultimately be limited by clearance problems at the H10 septum as seen from Eq. (4).

The above formulation neglects the variation of tune ν, and thus Ψ, with momentum in the AGS. Also, the momentum compaction function is changed in the perturbed machine which means that the phase space motion of the equilibrium orbit is not simply described by $x'_{EO} = -(\alpha/\beta)\, x_{EO}$ as in the unperturbed machine. We therefore made computer calculations of the separation at H10 using the AGS ray-trace program BEAM[7] which contains the appreciable machine non-linearity at the design momentum of 29 GeV/c. The results are given in Fig. 3 for 4 momentum groups. The clearance is in good agreement with the estimates of linear theory for this case; however, in other cases where the septum and ejector are separated by larger phase shifts than for E10 → H10, we see appreciable discrepancies with linear theory.

III. Orbit Deformations

The function of the fast orbit deformation is to move the beam adjacent to the septa at E10, H10 and I10, which are positioned at the injection aperture of the machine (about 2 in. from the central orbit). Since the SEB is assumed to be on prior to fast extraction, the orbits are contained between $\nu_H = 8\text{-}2/3$ and 9 which imposes several constraints on the fast bumps: ν_H must not decrease if the SEB-exciting sextupoles are on, and the deformation of the orbits near $\nu_H = 9$ (low momentum, inside orbit) must not be further increased by perturbations introduced by the bumps. We have considered two configurations of backleg winding bumps (BLWB).

Method A

We center a $\lambda/2$ BLWB at each of the three FEB septa and energize three additional inward $\lambda/2$ bumps to compensate for the $\Delta\nu \approx -.14$ ν-shift caused by the primary bumps. The compensating bumps are superimposed on the existing three $\lambda/2$ outward SEB bumps centered at F7, G10 and H20 and thus "cancel" the SEB bumps without causing an objectionable inward excursion and thus beam loss of low momentum protons. The cancelling bumps also aid in suppressing the slow beam by moving the beam away from the SEB septa.

The orbits resulting from the 6 FEB and 3 SEB bumps are shown in Fig. 4 for a momentum near the 8-2/3 resonance and .6% lower momentum. The low momentum orbit at $\nu_H = 8.90$ is seen to be highly deformed, with peak-to-peak oscillations of 5.2 in. which exceed the available aperture in the AGS. This orbit can be corrected with the aid of additional dipoles. In Fig. 5 we show an example of an orbit corrected by two pairs of AGS magnets excited with backleg windings and separated by approximately $\lambda/4$. The correction magnets are located downstream of the last (I10) FEB bump. An iterative technique is used to calculate the dipole strengths required to restore the beam to the unperturbed orbit. The corrected low momentum orbit has a maximum inward excursion of 1.9 in. In Fig. 5 the strength of the FEB "cancelling" bumps has been increased to assure that the ν shift is positive near 8-2/3. We note that, because of the small width of the 8-2/3 resonance, we can effectively move the entire beam out of its influence by a small ($\approx .02$) ν increase. We also point out that the oscillations from low momentum orbits can be mitigated by pulsing the AGS superperiod sextupoles and thus decreasing $d\nu/dp$.

The large oscillations in the orbits of Fig. 4 result from the dipole and quadrupole perturbations introduced by the bumps, and the proximity of the tune to the integral and half-integral resonances at $\nu_H = 9$. The dipole errors arise from two effects: the deviation of the BLWB from a perfect $\lambda/2$ separation, and the non-linearity of the AGS field. Consider first the 9th harmonic component of the orbit oscillation from dipole errors[3] due to one $\lambda/2$ bump (4 magnets):

$$\Delta x = \frac{\beta^{\frac{1}{2}}\nu_e^{\,i\nu_0\phi}}{2\pi(\nu^2 - \nu_0^2)} \sum_1^4 f_i \ell_i \beta_i^{\frac{1}{2}} e^{-i\nu_0\phi_i} + \text{C.C.} \tag{5}$$

where $f_i = (\Delta B)_i/p$, ϕ is the azimuthal angle Ψ/ν, and the ℓ_i are magnet lengths. We obtain $(\Delta x)_{\text{peak-to-peak}} = .66$ in. from Eq. (5) with $\nu = 8.9$ and $\nu_0 = 9$. The additional dipole error arises from the fact that the large deformation moves the beam over a large region of the AGS magnets, so that the effect of nonlinearities becomes appreciable. If we write for the vertical AGS field

$$B_Z = B_0 (1 + \epsilon_1 x + \epsilon_2 x^2) \tag{6}$$

with coefficients $\epsilon_1 = .10$ in.$^{-1}$ and $\epsilon_2 = -7 \times 10^{-4}$ in.$^{-2}$, where ϵ_2 was inferred from ν_H vs R measurements,[8] and if we assume that the orbit deformation between magnet pairs of the $\lambda/2$ bump is sinusoidal, i.e. $x = A \sin \nu_0\phi$, then the orbit oscillation around the remainder of the machine is

$$\Delta x = \frac{\beta^{\frac{1}{2}}\nu^2 e^{i\nu_0\phi}}{2\pi(\nu^2 - \nu_0^2)} \int_0^{\pi/\nu_0} \beta^{3/2} f e^{-i\nu_0\phi}\, d\phi + \text{C.C.} \tag{7}$$

where $f = \epsilon_2 B_0 A^2 \sin^2 \nu_0\phi/p$. We obtain from Eq. (7), using $A = 1.8$ in. and an average $\beta = 600$ in., $(\Delta x)_{\text{peak-to-peak}} = 1.0$ in. Since the amplitudes from Eq. (5) and (7) add, and the amplitudes from the other $\lambda/2$ bumps add in quadrature, the observed ~ 5 in. amplitude from Fig. (4) is not unreasonable.

The ν-shift associated with the $\lambda/2$ BLWB can similarly be explained by gradient errors within the AGS magnets and by non-linearities. For a $\lambda/2$ bump we can write[3]

$$\Delta\nu = \frac{1}{4\pi}\sum_1^4 k_i\beta_i\ell_i + \frac{1}{4\pi}\int_0^{\pi} k(\Psi)\,\beta(\Psi)\,d\Psi \tag{8}$$

where $k_i = (\Delta G)_i/p$, $k(\Psi) = 2\epsilon_2 B_0 A \sin\Psi/p$ and $(\Delta G)_i$ are the gradient errors within magnets with backleg windings. We obtain $\Delta\nu \approx -.05$ from Eq. (8) with $\sim 90\%$ of the ν-shift coming from the second term. This estimate of $\Delta\nu$ is consistent with the computed values of $\approx -.14$ for three $\lambda/2$ bumps.

Finally, we note that gradient errors from the BLWB increase the width of the stopband at $\nu = 18/2$ and thereby increase the β function oscillations[9] for orbits near the stopband. We can estimate the stopband width from one $\lambda/2$ bump as[3]

$$\delta\nu = \frac{1}{2\pi}\left|\sum_1^4 k_i\beta_i\ell_i e^{2i\Psi_i} + \int_0^{\pi} k\beta^2 e^{2i\Psi}\,d\Psi\right| \approx .03. \tag{9}$$

Computer calculations give for the total stopband width with all bumps energized: $\delta\nu \approx .1$. This results in a 30% increase in amplitude of betatron oscillations for the orbit at $\nu_H = 8.9$. The stopband also increases the orbit oscillations near $\nu_H = 9$ by increasing the β-function. We note that even if pure dipoles rather than powered backleg windings were used to produce the orbit

deformations, we would still have a large gradient stopband at $\nu_H = 9$ from the second term in Eq. (9).

Method B

Only fast $\lambda/2$ bumps centered at E10, H10 and I10 are used. We require that the SEB sextupoles be turned off during fast extraction. The horizontal tune of the high momentum orbit shifts from 8.67 to 8.55 while the low momentum orbit shifts to $\nu_H = 8.80$. The orbits are shown in Fig. (6). Since we are no longer near $\nu_H = 9$ the horizontal orbits are reasonably well behaved. However, ν_V for the high momentum particles shifts up to $\nu_V \approx 8.99$; thus we require that the superperiod quadrupoles be pulsed to shift ν away from the $\nu_H = 8\text{-}1/2$ and $\nu_V = 9$ resonances. The method requires that the 26 θ sextupole component in the ring be small since we are shifting part of the beam through the $\nu_H = 8\text{-}2/3$ non-linear resonance. The principle source of sextupole error is in the magnets with powered backleg windings. We estimate that the strength of the 26 θ sextupole error will be [10]

$$g = \left| \sum_{1}^{24} \frac{(\Delta B)_i \, \ell_2}{\rho} \ell_i e^{i26\phi_i} \right| \approx 0.2 \times 10^{-4} \text{ in.}^{-2} \quad (10)$$

which is small compared to the $g = 4 \times 10^{-4}$ in.$^{-2}$ introduced by the SEB sextupoles. By pulsing two independent sets of extraction sextupoles we can ensure a sufficiently small 26th harmonic as the beam moves through the resonance. We favor Method B since fewer orbit bumps are required and dipole orbit corrections do not appear necessary.

IV. Expected Beam Losses on Hyper Thin Septum

We have calculated[11] septum losses using a Monte Carlo technique by selecting proton coordinates at random from the phase space distribution of Fig. 2 and following the particles through either a solid foil electrostatic septum or an array of wires[12] parallel to a high voltage electrode. For a wire septum with wire radius ρ, wire spacing a and gap b relative to a plane at voltage V, the potential is known[13] and can be shown to give a nearly uniform field within the septum of strength $\mathcal{E} \approx (V/b)f$ where

$$f = 1/(1 + \frac{a}{2\pi b} \ell n \frac{a}{2\pi\rho}) \quad (11)$$

with f near unity. Protons strike the septum either at its upstream end or along its length. Within the array, proton scattering angles are selected randomly[14] from a Moliere[15] multiple-coulomb scattering distribution. In addition, elastic proton-nucleus scattering angles are selected from a distribution constructed from the differential cross section given by an optical model calculation.[16] Finally, protons are absorbed with a probability derived from the approximate interaction cross section [17] $\sigma_a \approx 43 \, A^{0.69}$ mb, where A is the atomic weight. The numerical results give a loss from scattering and absorption of 0.1% per turn for a .002-in. diam. tungsten wire array with a = 2 mm and length L = 2.25 m. The loss for a Cu foil septum of the same thickness and length is 0.8% per turn. Thus, for fractional turn extraction, beam losses will be negligible for either septum. For multiturn extraction, which we eventually plan to achieve, the factor of 8 smaller losses for the wire array will be significant. During initial beam tests it may be necessary to operate with a .010-in., 26-in. long Cu septum magnet at E10; the losses for this septum will be 6% per turn. We then plan to augment the copper septum with a 60-in. long electrostatic wire septum as an interim, hybrid straight section. The loss for this situation will be $\sim$ 0.9% per turn. For the hybrid straight section we calculated the losses for various wire materials, wire diameters, wire spacings and septum voltages. For samples of 10^5 protons, the results are (NABS = number absorbed, NSCAT = number diffraction scattered, NTARG = number lost in downstream septum, and L = loss):

Wire Material	Z	NABS	NSCAT	NTARG	L(%)
Be	4	38	24	1305	1.37
Aℓ	13	41	26	1264	1.33
Fe	26	69	73	1048	1.19
Cu	29	78	64	1054	1.20
Mo	42	74	76	955	1.10
W	74	104	101	794	1.00

a = 2mm, 2ρ = .002 in., V = 100 kV

W Wire Dia. 2ρ (inch)	NABS	NSCAT	NTARG	L(%)
.002	104	101	794	1.0
.004	373	393	543	1.3
.006	828	807	397	2.0
.008	1118	1063	202	2.4
.010	1140	1163	119	2.4

a = 2mm, V = 100 kV

W Wire Spacing a (mm)	NABS	NSCAT	NTARG	L(%)
1	155	165	516	.84
2	104	101	794	1.00
3	32	43	932	1.01
4	39	39	1159	1.24
5	33	25	1363	1.42

2ρ = .002 in. V = 100 kV

Septum Voltage (kV)	NABS	NSCAT	NTARG	L(%)
60	129	137	1788	2.05
70	143	135	1601	1.88
80	112	118	1238	1.47
90	108	100	1014	1.20
100	104	101	794	1.00

a = 2mm, 2ρ = .002 in. wire material W

The losses show a significant increase between .004 and .006 in. diam., a gradual decrease with increasing Z, an increase with larger wire spacing due to a decrease in deflecting field (decrease in f of Eq. (11)), and significant decreases with higher voltage.

V. Description of Components

The beam kickers will be single turn, full aperture ferrite dipoles, 33 in. long and with a 6 in. x 2-3/4 in. aperture. A capacitor bank will be discharged into the magnet through a deuteron thyratron to attain a peak current of 5000 A from a 1.75 μsec half-sinusoid waveform. The resulting 870 G field will produce a .75 mrad deflection, giving .4 in. displacement at the HTS. For full extraction of the AGS beam in three turns, we will add additional capacitor-switch systems to attain $\sim$ 15,000 A in 8 μsec. The kickers are separated by $\sim$ 3/2 λ to obtain a nearly local bump in the vicinity of the HTS. With a third, correction kicker in straight section D15, we can attain an ideal local bump.

The H10 EM septum will be built in two sections of length $\ell_1 = 25.5$ in. and $\ell_2 = 56.5$ in. To obtain the inward, -3 mrad, deflection for ejection at I10, the septum units will be powered with opposite polarity. For ejection at H10, the septum will deflect by + 22 mrad. The septum is .090 in. Cu, edge-cooled and with a 1 in. vertical gap. The peak current of 21,000 A will be obtained from a capacitor-discharge power supply with $\approx$ 1 msec half-sinusoid waveform. The unit will be capable of pulsing 4 times at 100 msec intervals. The .010 in., 26 in. long Cu septum required for the E10 hybrid straight section will be of similar design and capable of 1.2 mrad deflection. The electrostatic HTS upstream of the .010 in. Cu septum in E10 will be

1.5 m long with a 1 cm gap. At $\mathcal{E}$ = 100 kV/cm we should attain .5 mrad deflection.

Some operational experience has been gained from a prototype, 2.25 m long tungsten wire electrostatic septum recently installed in the AGS. The wires are .004 in. diam. at 2 mm spacing and the septum has held over 100 kV across a 1 cm gap in bench tests. The electrode is polished titanium and the straight section pressure is not higher than 1 x 10^{-7} torr. In the AGS we find that circulating beam losses occur for V $\gtrsim$ 10 kV when the machine tune crosses ν_H = 8-1/2 near injection. We believe that the gradient error causing these losses is due to an excessive ion density in the straight section, resulting from ion bombardment of the cathode with subsequent emission of secondary electrons which can penetrate the grid. Efforts are in progress to diminish the ion density and correct the gradient error. At reduced AGS intensity ($\sim$ 8 x 10^{11} ppp) we have observed beam separation of the expected magnitude on scintillating screens.

Acknowledgments

We thank A. Maschke, C. Germain, S. Senator, M. Fruitman, M.Q. Barton, Th. Sluyters, and J. Herrera for numerous suggestions regarding the hyper thin septum, and E. Forsyth and M. Fruitman for design studies of fast kickers. We are grateful to G. Bennett, A. Tranis, L. Repeta and J. Lancaster for design and planning of beam components. We acknowledge the efforts of H. Hsieh and A. Soukas in design studies for septum magnets and power supplies, of G. Bagley and F. Pallas for backleg winding development, of J. Schuchman and A. Bertsche for design of vacuum and positioning components, and J. Curtiss for instrumentation. We thank G.K. Green, D. Berley, R. Shutt, and H. Foelsche for discussions on the implications of the shaving method for the AGS experimental program. We thank G. Parzen and K. Jellett for field calculations for the electrostatic septum and kicker magnets.

References

1. G.K. Green, BNL Accel. Dept. Int. Rep. GKG-6 (1962).
2. E. Forsyth and C. Lasky, BNL Accel. Dept. Int. Rep. BNL-910 (1965).
3. E.D. Courant and H.S. Snyder, Ann. Phys. 3, 48 (1958).
4. M.Q. Barton, private communication (1968).
5. L. Blumberg, M.Q. Barton, J. Fox, J. Glenn, and L. Repeta, BNL Accel. Dept. Int. Rep. AGS DIV 69-12 (1969).
6. L. Blumberg, M.Q. Barton, G. Bennett, J. Fox, J. Glenn, H. Hsieh, R. Nawrocky, and A. Soukas, Proc. U.S. Nat'l. Part. Accel. Conf., IEEE Trans. Nucl. Sci. NS-16, No. 3, 234 (1969).
7. For the FORTRAN IV version of E.D. Courant's AGS Orbit program, see G.H. Morgan, BNL Accel. Dept. Int. Rep. GHM-1 (1966).
8. M. Month, E. Gill and E. Raka, Nucl. Instr. Meth. (in press).
9. J. Herrera and M. Month, BNL Accel. Dept. Int. Rep. AGS DIV 69-2 (1969).
10. M. Month, BNL Accel. Dept. Int. Rep. AGSCD-17 and AGSCD-19 (1967).
11. L. Blumberg and F. Krausz, BNL Accel. Dept. Int. Rep. AGS DIV 71-1 (1971).
12. A. Maschke, Proc. 7th Int. Conf. on High Energy Accelerators, Yerevan, USSR, p. 576, Vol. 1 (1969).
13. P. Morse and H. Feshbach, Methods of Theoretical Physics, Vol. II (McGraw-Hill, 1957), p. 1237.
14. G. Marmer, ANL Accel. Dept. Int. Rep. GJM-1 (1968).
15. G. Moliere, Z. Naturforsch. 2a, 133 (1947) and 3a, 78 (1948). See also H. Bethe and J. Askhin in Experimental Nuclear Physics, Ed., E. Segre (John Wiley & Sons, Inc., 1952), Vol. 1, p. 282.
16. Fernbach, Serber and Taylor, Phys. Rev. 75, 1352 (1949).
17. D. Keefe and M. Scolnick, LRL Rep. UCRL-16830, Vol. 2 (1966).

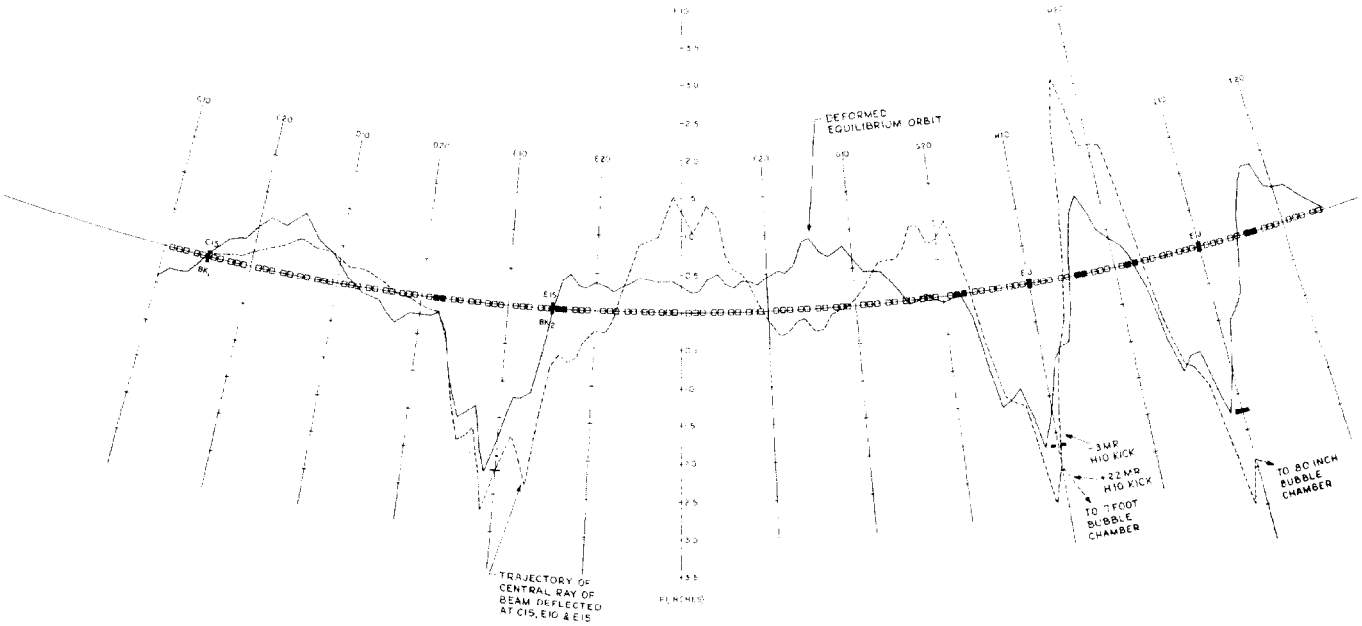

Fig. 1. Configuration of fast beam components in the AGS ring. The deformed equilibrium orbit resulting from $\lambda/2$ backleg winding bumps is indicated by the solid curve. The trajectory of the central ray deflected by the beam kickers and E10 and H10 septum magnets is given by the dashed curve. The AGS magnets used for producing the FEB orbit deformations are darkened. BK_1 and BK_2 refer to the beam kickers at C15 and E15.

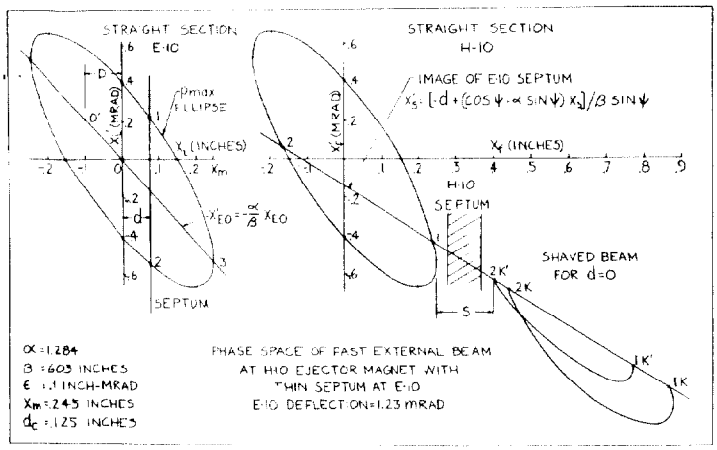

Fig. 2. Beam ellipse at E10 and "shaved" beam at H10 ejector magnet as described by Eqs. (1) to (4) in text. The shaved beam has been displaced downward for illustration purposes.

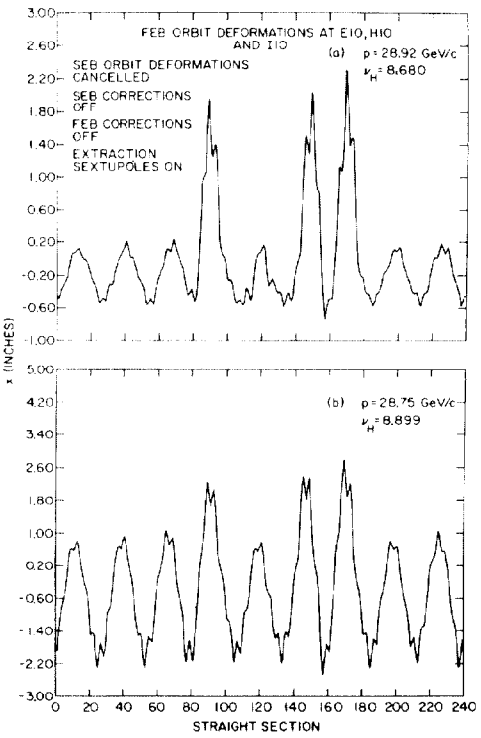

Fig. 4. Fast external beam orbit deformations at E10, H10, and I10. The SEB orbit deformations are cancelled with fast orbit deformations using the backlegs of adjacent AGS ring magnets. The SEB sextupoles and superperiod quadrupoles are on. No correction windings are used.

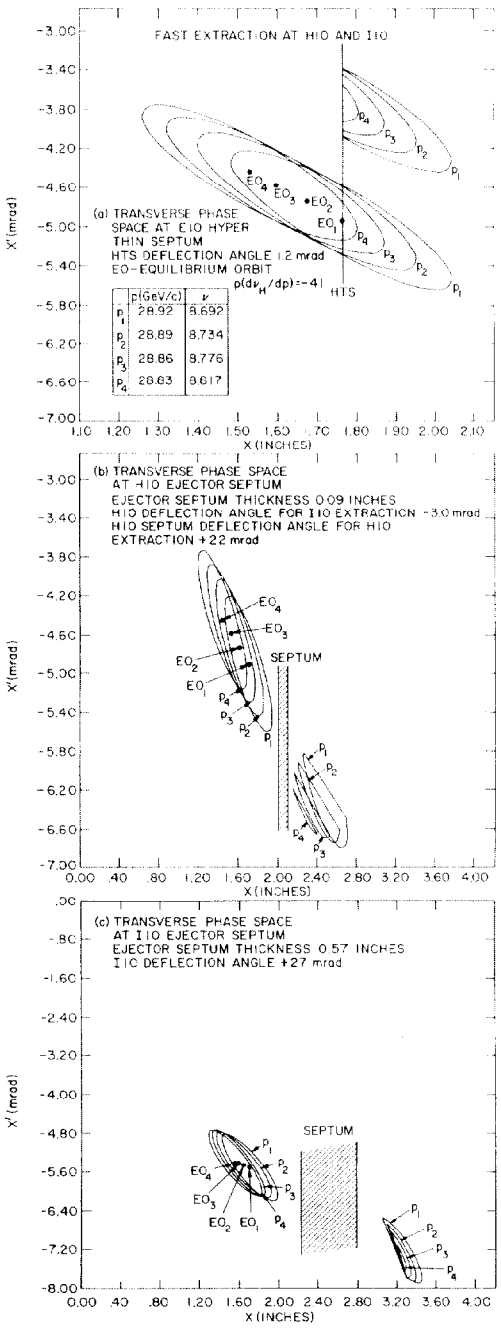

	p(GeV/c)	ν
p_1	28.92	8.692
p_2	28.89	8.734
p_3	28.86	8.776
p_4	28.83	8.817

Fig. 3. Fast extraction at H10 and I10. Orbit corrections, extraction sextupoles, and superperiod quadrupoles are on. The SEB orbit deformations are overcompensated by 25% with fast orbit deformations.
(a) Beam "shaving" by the hyper thin septum at E10.
(b) Separation at the H10 septum.
(c) Separation at the I10 septum.

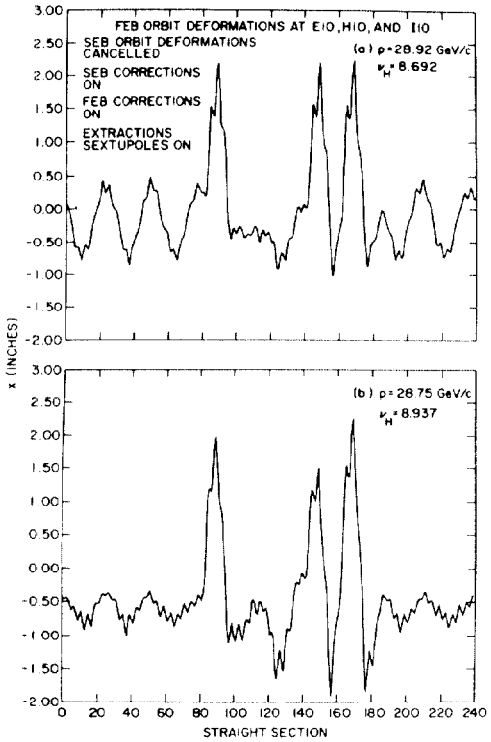

Fig. 5. Fast external beam orbit deformations at E10, H10, and I10. The SEB orbit deformations are overcompensated by 25% with fast orbit deformations to obtain a slight upward ν shift. The extraction sextupoles and superperiod quadrupoles are on. Additional backleg windings are used for both SEB and FEB orbits to correct the low momentum (inside) orbit.

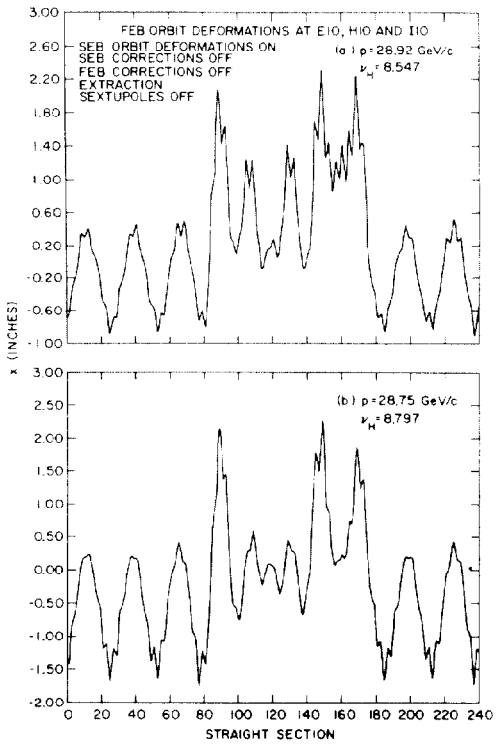

Fig. 6. Fast external beam orbit deformations at E10, H10, and I10. The SEB orbit deformations are present and not compensated. No correction windings are used and the extraction sextupoles are off. The superperiod quadrupoles are on and keep the horizontal ν value above $8\frac{1}{2}$.